IFUSP/P-117

THE THEORY OF THE GLORY

by

V.Khare
" " "
Max-Planck-Institut für Strömungsforschung, Göttingen, W.Germany

and

H.M.Nussenzveig*
Instituto de Física, Universidade de São Paulo, SP., Brasil

THE THEORY OF THE GLORY

by

V. Khare
Max-Planck-Institut für Strömungsforschung, Göttingen,
West Germany

and

H. M. Nussenzveig*
Instituto de Física, Universidade de São Paulo, Brasil

1. Introduction

Early one morning in 1735, a small group of people were gathered on top of a mountain in the Peruvian Andes. They belonged to a French scientific expedition, led by Bouguer and La Condamine, that had been sent out to measure a degree of longitude; a Spanish captain named Antonio de Ulloa accompanied them. What they saw on this occasion was, according to Bouguer[1], "a phenomenon which must be as old as the world, but which no one seems to have observed so far... A cloud that covered us dissolved itself and let through the rays of the rising sun... Then each of us saw his shadow projected upon the cloud... The closeness of the shadow allowed all its parts to be distinguished: arms, legs, the head. What seemed most remarkable to us was the appearance of a halo or glory around the head, consisting of three or four small concentric circles, very brightly colored, each of them with the same colors as the primary rainbow, with red outermost...". Ulloa, who gave a similar description and also drew a picture of what he observed, added: "... The most surprising thing was that, of the six or seven people that were present, each one saw the phenomenon only around the shadow of his own head,

and saw nothing around other people's heads...".

During the nineteenth century, many observations of the effect were made from the top of the Brocken mountain in Germany, and it became known as the "spectre of the Brocken". It also became a favorite image among Romantic writers[2]; it was celebrated by Coleridge in "Constancy to an Ideal Object". Cellini was deeply affected by his own mystical experience[3] with the "Heiligenschein", a superficially similar optical effect with an entirely different origin[4]. One may well wonder about iconographic and hagiographic implications.

Other sightings of the glory were made from balloons (around the shadow of the balloon on the clouds), and nowadays it is most commonly seen from airplanes. Recently, some beautiful color photographs of the effect have been reproduced[5].

C.T.R. Wilson invented the cloud chamber after observing the glory from the top of the Ben Nevis mountain in Scotland because, in his own words[6], these "...marvelous optical phenomena... greatly arose my interest, and led me to desire to imitate them in the laboratory." However, he did not achieve his original aim.

The glory is generally observed over thin clouds or mist, formed out of very tiny water droplets. In terms of the dimensionless size parameter $\beta = ka$ (k = wave number; a = droplet radius), the most favorable range for the observation of natural glories seems to be from $\beta \sim 10^2$ to $\sim 10^3$, with an average value[7] of about 160, corresponding to a $\sim 14\mu$.

The appearance of the glory rings varies considerably from one observation to another, and sometimes even during a single observation. As many as five sets of rings have been seen. That "each one is his own saint" is most easily explained: the effect is contained within a narrow solid angle, of the order of at most a few degrees around the backscattering direction ; the only function of the shadow is to identify this direction. There are indications that the glory rings are strongly polarized.

More than two centuries after the first recorded observation, an adequate physical explanation of this beautiful effect was still lacking, in spite of the availability of Mie's exact mathematical solution[8] since the beginning of this century.

This is not so surprising, since the glory is indeed a very complicated effect.

In the present work, after a brief review of the various theories that have been proposed, we discuss the recent explanation of the glory[9] based on the theory of complex angular momentum. It is a pleasure to dedicate this paper to Elliott W. Montroll, whose broad range of interests has also included Mie scattering theory, on the occasion of his sixtieth birthday.

2. Early Theories

The first attempts to give a theoretical explanation of the glory were based on an apparent analogy with another meteorological effect, the diffraction coronas often observed around the moon or the sun. These are due to diffraction by water droplets in the clouds, and their angular distribution is given by the Airy pattern characteristic of an obstacle with a circular rim: $J_1^2(\beta\theta)/\theta^2$, where J_1 is Bessel's function of order one and θ is the scattering angle. However, since this gives rise to a forward diffraction peak rather than a backward one, the reversal of the direction of propagation of the scattered light must still be explained. The earliest theories, due to Fraunhofer and to Pernter[1], proposed that the reversal took place by reflection from the clouds. Such theories are untenable, not only because of the implausibility of a regular reflection from a cloud, but also because they would not account either for the angular distribution (quite different from the Airy pattern) or for the polarization of the glory rings.

In 1923, B.Ray concluded[10], on the basis of experiments with artificial clouds, that the glory is produced individually by each water droplet in its own backscattering. This was confirmed by later results.

Ray also proposed to explain the glory in terms of interference between axial rays directly reflected from the outer surface of the droplet and those which penetrate into it and are reflected internally from the back surface. However, even

if one takes into account the whole series of multiple internal reflections of such axial or paraxial rays, the resulting intensity is far too small to explain the observed effect[11,12]. Similar remarks apply to Bricard's treatment[13].

Bucerius[14] proposed an explanation in terms of "backwards diffraction", an effect similar to the forward diffraction peak but giving rise to a backward dip (dark central disc) rather than a peak. This would again disagree with the observed intensity, angular distribution and polarization.

3. Van de Hulst's Theory

One can try to save geometrical optics by looking for non-paraxial rays that are backscattered after one internal reflection. A ray of this type, such as ABCDE in fig. 1, would be called a "glory ray". It was shown by Van de Hulst[15] that two peculiar effects associated with such rays would lead to scattering anomalies.

As is illustrated in fig. 1 by tracing the paths of neighboring rays, a portion of a plane incident wavefront ii' is transformed (for a generic scattering angle θ) into a portion of spherical transmitted wave front tt' that seems to emanate from the virtual focus F. For $\theta=\pi$, however, due to the axial symmetry, the whole picture must be rotated around the axis, so that, instead of a single focus (virtual point source), we get a whole focal circle (virtual ring source), giving rise to toroidal wave fronts. This leads to axial focusing, the first of Van de Hulst's two effects: along the axis, the rays emanating from the focal circle interfere constructively, producing an intensity enhancement (in geometrical optics, the axis would be a focal line, along which the intensity would be infinite, a kind of backwards Poisson spot).

The second peculiar effect has to do with polarization. Parallel and perpendicular polarizations with respect to the scattering plane (the plane containing the directions of incidence and of observation) are independently scattered for a generic direction θ. However, for $\theta=\pi$ (as well as $\theta=0$), the scattering plane is not defined. Thus, a parallel component with respect to the plane of fig. 1 appears as perpendicular

component after a 90° rotation around the axis, and the resultant backscattered waves vibrate in the same direction; their interference thus simulates an interference between parallel and perpendicular polarizations. Van de Hulst calls this the cross-polarization effect.

In the neighborhood of $\theta=\pi$, two scattered rays would emerge in each direction, arising from incident rays close to but on different sides of the glory ray: their interference would give rise to the glory rings.

Unfortunately, as Van de Hulst pointed out, there is a basic flaw in the above explanation: for the refractive index $N\approx 1.33$ of water, glory rays of the type drawn in fig. 1 do not exist; they would only be present[7,11] for $\sqrt{2} < N < 2$ (e.g., for glass spheres). For water, the largest deviation attained for rays of the class shown in fig. 1 corresponds to tangentially incident rays, which reemerge about 14° away from the backward direction. How can this 14° gap be bridged?

Van de Hulst suggested that this might be a diffraction effect that would take place within the favorable range of β. Specifically, he proposed as a likely mechanism the generation of surface waves ("creeping waves") both at points of tangential incidence, as at T_1 (fig.2), and at points of total internal reflection[16], such as B and D (fig. 2); such waves reenter the sphere at the critical angle, as at A and C, giving rise to the "shortcuts" AB and CD. The surface wave portions such as T_1A, BC and DT_2 would add up to the required 14°.

At the time this theory was proposed, it could not be placed on a quantitative basis leading to definite predictions for the scattered intensities, so that its validity could not be tested.

4. Exact Mie Results

The exact solution of the problem of the scattering of a monochromatic plane electromagnetic wave by a homogeneous sphere in the form of a partial-wave expansion was given by Mie[8] in 1908. Let the electric field of the incident wave be given by

$$\underset{\sim}{E}_{in} = \exp(ikz)\,\hat{\underset{\sim}{x}}\,. \tag{1}$$

The corresponding scattered electric field is

$$\underset{\sim}{E}_{sc} \approx \left[S_1(\beta,\theta)\sin\varphi\ \hat{\underset{\sim}{\varphi}} - S_2(\beta,\theta)\cos\varphi\ \hat{\underset{\sim}{\theta}} \right] \times \exp(ikr)/ikr \qquad (r \to \infty), \tag{2}$$

where the scattering amplitudes S_1 and S_2 are associated with perpendicular and parallel polarization, respectively.

The scattering is completely characterized by three real quantities: the two polarized intensities

$$i_j(\beta,\theta) = |S_j(\beta,\theta)|^2 \qquad (j = 1,2),$$

which determine the differential cross-sections, and the phase difference

$$\delta(\beta,\theta) = \arg S_1 - \arg S_2,$$

which determines the state of polarization of the scattered wave.

The Mie solution is of the form

$$S_1(\beta,\theta) = \frac{1}{2}\sum_{\ell=1}^{\infty}\left\{ \left[1 - S_\ell^{M}(\beta)\right] t_\ell(\cos\theta) + \left[1 - S_\ell^{E}(\beta)\right] p_\ell(\cos\theta) \right\}, \tag{3}$$

where t_ℓ and p_ℓ are angular functions of the associated Legendre type and S_ℓ^M, S_ℓ^E are S-matrix elements for magnetic and electric multipole waves of order ℓ, respectively; $S_2(\beta,\theta)$ is obtained by interchanging E and M; $S_\ell^{M,E}$ are complicated ratios of combinations of spherical Bessel and Hankel functions. Expect in near-forward and near-backward directions, the contributions from $t_\ell(\cos\theta)$ are dominant over those from $p_\ell(\cos\theta)$, so that S_1 is associated with magnetic polarization and S_2 with electric polarization.

If $\beta \gg 1$, the ℓth partial wave can be pictured in terms of incident rays with an impact parameter

$$b_\ell = (\ell + \tfrac{1}{2})/k \,, \qquad (4)$$

and only those partial waves with $b_\ell \lesssim a$ are significantly distorted, so that one must keep roughly $\sim\beta$ terms in the Mie series. Since β is very large in the range of interest, the partial-wave series provides essentially no insight into the physical effects that are responsible for the glory.

On the other hand, it can be employed in computer calculations, as a source of numerical data. Numerical studies of this type have been made by Bryant and coworkers[12,17] for the β-dependence of the glory intensity, and by Dave[18] for its angular distribution and polarization. In both cases, the results show extremely rapid and complicated fluctuations with all of the parameters: β, θ and N.

Bryant and coworkers computed the intensity at $\theta = \pi$ in the ranges $200.0 \lesssim \beta \lesssim 201.8$ and $500.0 \lesssim \beta \lesssim 501.0$ for $N = 1.333$, and in the range $3000.0 \lesssim \beta \lesssim 3001.4$ for $N = 1.333$ and for $N = 1.333 + 2 \times 10^{-6} i$. The results show the following features (see also figs. 8 to 10 below):

i) The backscattered intensity is a rapidly-varying, quasi-periodic function of β, with a quasi-period $\Delta\beta \approx 0.815$.

ii) Within a quasi-period, there is a relatively more slowly-varying background, showing about three humps per quasi-period.

iii) Superimposed on the humps, there are additional fluctuations, including some extremely sharp spikes, representing intensity variations by one to two orders of magnitude within a range $\delta\beta \sim 0.01$, corresponding to a change in droplet radius by a few thousandths of the wavelength!

iv) When a small absorptive term is included in the refractive index, the spikes tend to be smoothed down, but not the humps.

The relative contributions of different partial waves were also numerically investigated in terms of the "localization principle" (4), by plotting the growth of the sum of the Mie series as a function of the number of terms retained. The conclusions were:

v) The backscattered intensity arises predominantly

from incident rays very close to tangential incidence at the "edge" of the sphere.

vi) The contribution from axial and paraxial rays, as remarked above, is too small, by up to one order of magnitude or more, to account for the backscattered intensity.

Fahlen and Bryant[17] also made an experimental study of the backscattering of a focused laser beam from a single water droplet suspended from a glass fiber; the size parameter was in the range 10^3 to 10^4. In view of the continuous evaporation of the droplet, a plot of the backscattered intensity as a function of time reproduces its behavior as a function of β. The above-described features of the numerical computations are also apparent in the experimental results. Similar experiments were performed by M.J.Saunders[19], with much smaller droplets (β in the range from $\sim$50 to $\sim$300) suspended from submicroscopic spider threads.

Dave[18] computed the angular distribution and polarization for N = 1.342 near $\theta = \pi$ for β= 98.2, 196.3, 392.7 and 785.4. For the lower values of β, the first dark ring is only a small depression; this "haziness of the first dark ring" was also pointed out by Van de Hulst[7]. The outer rings tend to be parallel-polarized. For the higher values of β, perpendicular polarization predominates in the outer rings; for β = 785.4, the first bright ring is brighter than the central field. Thus, both the angular distribution and the polarization undergo considerable changes as a function of β.

5. The Watson Transformation

We are faced with the situation of having at hand the exact solution of the problem (Mie series), and yet being unable to understand its physical content. Even numerical work is difficult and costly, in view of the extremely rapid variation with all the parameters: e.g., in the computations described above, calculated points were spaced 0.001 apart in β, and double-precision arithmetic, with 22 significant figures, was employed.

The first successful attempt to extract the physics

contained in the partial-wave series at high frequencies was the Watson transformation, which resulted from the work, among others, of Poincaré and Watson[20], around 1910. The motivation was to find out how radio waves overcome the Earth's curvature (this was before the discovery of the ionosphere!), so that the main concern was with the neighborhood of the Earth's surface, in the shadow zone of the transmitter. The idea was to substitute the partial-wave series by an equivalent contour integral in the λ-plane, where $\lambda = \ell + \frac{1}{2}$ can be interpreted, according to (4), in terms of angular momentum. One gains the freedom of path deformation in the complex-angular-momentum plane. This can be employed to obtain rapidly convergent asymptotic estimates, by suitable choosing a path to concentrate the dominant contributions in a few "critical points", rather than having them distributed among many partial waves.

In Watson's case (shadow region), the critical points were complex poles λ_n, which nowadays would be called Regge poles. Their imaginary part, associated with angular damping, grew quite rapidly with n, so that only a few poles closest to the real axis had to be considered, leading to a rapidly-convergent "residue series". Its terms are "creeping waves" generated at the edge of the sphere (points of tangential incidence in fig. 2), which travel along the surface shedding radiation tangentially, so that $\mathrm{Im}\,\lambda_n$ represents radiation damping.

If one moves aways from the shadow into a lit region, Watson's original method breaks down. The procedure for dealing with this situation was discussed by Fock[21] around 1945 (for the work of some predecessors, cf.[20]). Besides Regge pole contributions, one must also consider what became known as the "background integral" in the λ-plane, which is now dominant. The critical points for this integral are saddle points $\bar{\lambda}_j$ which, when located on the real axis, are associated with geometrical-optic rays and give rise to the expected contributions therefrom; when additional terms are taken into account in the saddle-point method, one recovers the WKB series.

On the surface of the sphere, the transition between light and shadow takes place in a "penumbra region", and it

is described by a new mathematical function, the "Fock function"[21]. This is the region near the edge where creeping waves are generated; its angular width is of the order of $\beta^{-1/3}$. Fock's function interpolates smoothly between the geometrically lit (WKB) region and the creeping-wave region.

The method was applied not only to radio wave propagation[21,22] and to the scattering by impenetrable spheres, but also to the transparent sphere problem[23,24,25]. Although significant advances were made, e.g. in the discussion of creeping waves and of Fock's penumbra region, only a few disconnected regions, separated by wide gaps, were treated. While contact was established with previously known approximations, like Airy's theory of the rainbow[23], the results did not go beyond them. In the glory problem, some justification was provided to Van de Hulst's conjectures about surface waves, but quantitative results were still lacking.

6. The Modified Watson Transformation

An improved version of Watson's method, developed[26] in 1965, finally made it possible to derive from the partial-wave expansion the asymptotic behavior of the solution at any distance from the sphere and in any direction. The new method was applied to the scattering of a scalar field by a impenetrable sphere[26] and by a transparent sphere[11], including a discussion of the rainbow and the glory. It was later extended to electromagnetic scattering[27], and the results were compared with the exact Mie solution both for the rainbow[28] and for the glory[9]. We refer to the original papers, as well as to a previous survey[29], for a detailed discussion of the method. We are concerned here only with the aspects that are relevant for the explanation of the glory.

The modified Watson transformation is based on the application of Poisson's sum formula[30]

$$\sum_{\ell=0}^{\infty} \varphi\left(\ell+\tfrac{1}{2},\beta,\theta\right) = \sum_{m=-\infty}^{\infty} (-)^m \int_0^{\infty} \varphi(\lambda,\beta,\theta)\, e^{2im\pi\lambda}\, d\lambda, \qquad (5)$$

followed by completion of a symmetric path about the origin and its judicious deformation in the λ-plane. This deformation, which must be performed differently in different angular regions, also leads to Regge pole contributions and to background integrals, usually dominated by saddle-point contributions.

A saddle point on the real axis is also a stationary-phase point in (5), thus characterizing an extremal path, i.e., a geometrical-optic ray (classical orbit, in particle language). The integer m in (5) has the topological significance of a winding number, corresponding to the number of turns performed by a path around the center of the sphere. The Poisson sum formula has also been employed as the starting point in semi-classical approximations to scattering; the connection between this approach and Feynman's path integral method has been discussed by Berry[31].

Regge poles for a transparent sphere are of two quite different types. One of them, similar to Watson's, is associated with surface ("creeping") waves; as shown by Keller[32], such contributions can also be given an extremal characterization, in terms of "diffracted rays". The other type of Regge poles is associated with resonances. Since resonances appear in many partial waves at high frequencies, one finds lots of poles of this type clustered close to the real axis, spoiling the rapid convergence of the residue series.

A way out of this difficulty had already been pointed out by Van der Pol and Bremmer[23], who applied an expansion first employed by Debye[33] in the case of a circular cylinder. The interaction with the sphere of each spherical multipole wave can be broken up into a series of interactions at the surface, much in the same way as the problem of a Fabry-Perot interferometer can be solved in terms of a series of multiple internal reflections. One reflecting surface is the surface of the sphere; the other one degenerates into a point, the center of the sphere, which simulates a perfect reflector.

The expansion is obtained by representing the S-matrix elements $S_\ell^{E,M}(\beta)$ in (3) in terms of a geometric series

$$\frac{1}{1-\rho} = \sum_{p=1}^{P} \rho^{p-1} + \frac{\rho^P}{1-\rho} , \qquad (6)$$

where $\rho(\lambda,\beta)$ is, apart from a phase factor, the internal spherical reflection coefficient for multipole waves of order ℓ ($\lambda = \ell + \frac{1}{2}$). This leads to a corresponding decomposition of the scattering amplitudes (3),

$$S_j(\beta,\theta) = S_{j,0}(\beta,\theta) + \sum_{p=1}^{P} S_{j,p}(\beta,\theta) + \text{remainder} \quad (j=1,2), \qquad (7)$$

where each $S_{j,p}$ has the form of a partial-wave series. This is the Debye expansion: $S_{j,0}$ represents direct reflection from the surface, and $S_{j,p}$ ($p \geq 1$) represents transmission through the surface after p-1 internal reflections.

The modified Watson transformation can now be applied to each term of the Debye expansion. The associated poles in the λ-plane, which will be called Regge-Debye poles, no longer cluster near the real axis: they are all of the surface-wave type, so that we regain rapid convergence of the residue series. The Regge-Debye poles are the same for all Debye terms; however, they are poles of order p+1 for the p^{th} term. Physically, although the resonances disappear from each term, their effects may become manifested in the sum of the series (as in the Fabry-Perot case).

For partial waves with associated impact parameter $b_\ell < a$ (cf. (4)), $|\rho|$ is essentially the Fresnel reflection coefficient at the corresponding angle of incidence, and this coefficient, for water, is very small until one gets close to grazing incidence. It is only near the edge (Fock's penumbra region) that $|\rho|$ gets close to unity. For $b_\ell > a$, although $|\rho|$ is very close to unity, the corresponding partial waves do not contribute to the scattering, because they are prevented by the centrifugal barrier from reaching the sphere, except again very close to the edge, where they can tunnel through the barrier. Thus, we expect that high-order terms in the Debye expansion may give significant contributions to the scattering only for partial waves in the edge domain, defined by

$$\beta - c\beta^{1/3} \lesssim \lambda \lesssim \beta + c\beta^{1/3} , \qquad (8)$$

where c is a numerical constant of order unity. This is the region near the top of the barrier in the effective potential where, for smooth potentials, orbiting effects take place[34]. In the present case, the effective potential has a cusp, as shown in fig. 3, but the edge domain still gives rise to effects similar to orbiting, as will be seen below. The numerical studies mentioned above[12] indicate that the leading contributions to the glory arise from the domain (8).

7. Non-glory Regions

We discuss the results[11,27-29] obtained away from the near-backward region only to the extent that they are relevant to the theory of the glory. In these non-glory regions, the dominant contributions usually do not come from the edge domains, so that the rapid convergence of the Debye expansion follows from the damping effect of multiple internal reflections, and one may ordinarily stop at P=2 in (7).

i) Geometrical optics

At the level of geometrical optics, the p^{th} term of the Debye series is associated with rays that undergo p-1 internal reflections. For each p, the domain $0 \lesssim \theta \lesssim \pi$ is subdivided into angular sectors characterized by the number s of geometrical-optic rays of class p scattered in the same direction (s=0 for a dark sector). When the modified Watson transformation is applied to $S_{j,p}(\beta,\theta)$, each such ray is associated with a saddle point on the real λ-axis in (5). Different path deformations in the λ-plane are generally required in different angular sectors.

ii) Surface waves

The contributions from Regge-Debye poles represent surface waves, generated both at the edges of the sphere and following shortcuts through the sphere at the critical angle (fig. 2). The contribution from a Regge-Debye pole λ_n contains a factor

$$\exp(i\lambda_n\psi), \tag{9}$$

where Ψ is the total angle described along the surface; the damping factor $\mathrm{Im}\lambda_n$ represents the radiation damping associated with travel along a curved surface. For an internally incident ray at the critical angle, there are two possible types of interactions with the surface (fig. 4): (I) "Total" reflection ; (II) Critical refraction to the outside, followed by describing an angle φ as surface wave and by critical refraction into the sphere. Since φ may take any value and since we may have any combination of type-I and type-II "vertices", there are several classes of "diagrams" with p-1 vertices that contribute to a Debye term of order p.

At the boundaries between adjacent angular sectors, corresponding to changes in s (the number of rays in the same direction), geometrical optics would predict sharp discontinuities. Each of them is replaced by a transition region where diffraction effects become important. The following types of transition regions are found:

iii) Forward diffraction peak

This is the sector $0 \lesssim \theta \lesssim \beta^{-1}$, where the Airy diffraction pattern (cf.Sect.2) is dominant.

iv) Fock-type transitions

They are associated with the substitution of a real saddle point (geometrical ray) by a set of Regge-Debye poles (surface waves), interpolating smoothly between these two types of contributions. Their angular width is usually of the order of $\beta^{-1/3}$.

v) Rainbow regions

They are associated with the transformation of a pair of real saddle points into complex saddle points. At an extremum of the deflection function, one scattered ray "folds back" onto another one, leading to double coverage of one angular sector ("lit side"), whereas both rays are missing on the other side ("dark side"). In the λ-plane, this corresponds to a collision between two saddle points, which move towards each other along the real axis as the scattering angle approaches the rainbow angle from the lit side, come together at the rainbow angle, and then move apart in complex-conjugate directions on the dark side (fig.5).

When the ranges of two saddle points overlap, the ordinary saddle-point method can no longer be applied. Chester, Friedman and Ursell[35] have shown how to obtain a uniform

asymptotic expansion in this situation. The result for a typical rainbow term is of the form (cf. (25) below)

$$f(K,\theta)\left\{\left[p_0(\theta)+p_1(\theta)/K+\cdots\right]Ai\left[K^{2/3}\zeta(\theta)\right]\right.$$

$$\left.-K^{-1/3}\left[q_0(\theta)+q_1(\theta)/K+\cdots\right]Ai'\left[K^{2/3}\zeta(\theta)\right]\right\},\quad K=2\beta, \tag{10}$$

where Ai(z) is the Airy function, and the functions f and ζ, as well as the coefficients p_i, q_i, are determined by the two saddle points. Airy's classical theory of the rainbow is obtained by retaining only p_0 and by making the lowest-order approximations in the evaluation of f, ζ and p_0. The amplitude enhancement at the rainbow angle is of the order of $\beta^{1/6}$.

For the primary bow, which appears in the p=2 Debye term, it is found[28] that the corrections to the Airy approximation (arising mainly from q_0 in (10)) are small for S_1 (magnetic polarization), but quite large for S_2 (electric polarization). On the dark side of the rainbow, the Airy functions get rapidly damped; for large positive argument, we may employ the asymptotic expansion

$$Ai(K^{2/3}\zeta)\approx \exp\left(-\tfrac{2}{3}K\zeta^{3/2}\right)/2\sqrt{\pi}K^{1/6}\zeta^{1/4}\quad(K^{2/3}\zeta\gg 1), \tag{11}$$

which yields the exponentially damped contribution from the lower complex saddle point in fig. 5 sufficiently far from the rainbow angle. This contribution may be interpreted in terms of a "complex ray": the rainbow, as is well-known, is associated with a caustic[36], and complex rays appear on the shadow side of caustics[32], an effect that may be compared with quantum-mechanical tunnelling.

8. Application to the Glory

We now confine our attention to the immediate neighborhood of $\theta=\pi$ and we discuss some of the physical effects that are found in this neighborhood.

i) Cross-polarization

For $\theta=\pi$, one has

$$t_\ell(-1) = -p_\ell(-1) = (-)^\ell\left(\ell+\tfrac{1}{2}\right), \tag{12}$$

and the Mie series (3) becomes

$$S_1(\beta,\pi) = S^M(\beta) + S^E(\beta) = -S_2(\beta,\pi), \tag{13}$$

where the magnetic and electric contributions are now of the same order of magnitude. This is the cross-polarization effect mentioned by Van de Hulst (Sect.3); the effect actually extends over a small neighborhood of the backwards direction.

ii) Geometrical-optic terms

The paraxial-ray contributions to near-backward scattering include, besides the direct-reflection term (p=0), the geometrical-optic contributions from even values of p in (7), representing rays that are backscattered after p-1 internal reflections. Since the reflectivity at perpendicular incidence is very small, only p=2 need be taken into account. The combined effect of these two main terms is readily evaluated[11,27]; at $\theta=\pi$, it is of the form

$$S_{j,g}(\beta,\pi) \sim R\beta \qquad (j=1,2), \tag{14}$$

where the magnitude of R is of the order of the reflection coefficient at perpendicular incidence, i.e., $\sim 10^{-1}$; R is oscillatory in β, with a period of order unity, due to the interference between the directly reflected ray and the once-internally-reflected one. Within the range of β of interest, as has already been mentioned in Sect. 2, (14) gives only a small contribution to the intensity, in the form of a smoothly-varying background, which is totally unrelated with the glory.

For N≈1.33, non-paraxial geometrical-optic contributions can occur only for large p (cf. Sect. 2), where they are strongly damped by multiple internal reflections, except for incident rays in the edge domain; these, however, give rise to different effects, as will be seen below.

iii) Van de Hulst's term

This term (fig. 2) is the contribution of Regge-Debye poles for p=2, corresponding to surface waves that take two shortcuts through the sphere. The residue-series evaluation at $\theta=\pi$ leads to a result[11,27] of the form (cf. (9))

$$S_{j,res}^{(p=2)}(\beta,\pi) \sim c\,\beta^{4/3}\exp(-0.4\beta^{1/3}) \qquad (j=1,2), \tag{15}$$

where c is of order unity and only the lowest Regge-Debye pole is taken into account, so that (15) is to be understood only as an order-of-magnitude result.

In the relevant range of β, the contribution from (15) is several times larger than (14) and, for $\beta\sim10^2$, it is of the same order of magnitude as the glory amplitude[11]. Nevertheless, (14) and (15) together cannot account for the main features of the backscattered intensity (cf.Sect.4); higher-order Debye contributions must play an important role[11].

iv) Axial focusing

For all higher-order Debye terms, we may restrict our attention to "peripheral" contributions, i.e., those arising from incidence in the edge domain (8). All other contributions are strongly damped by multiple internal reflections, whereas in the edge domain the reflectivity is close to unity. This also agrees with the conclusions derived from numerical studies (Sect. 4(v)). In the complex λ-plane, therefore, all significant contributions arise from a neighborhood of $\lambda=\beta$.

Near the backward direction, (3) should be replaced[27] by a representation in terms of $t_\ell(-\cos\theta)$, $p_\ell(-\cos\theta)$. Setting

$$\theta = \pi - \varepsilon \quad , \qquad 0 \leqslant \varepsilon \ll 1 \quad , \tag{16}$$

we may employ Szegö's uniform asymptotic expansions[26]

$$p_{\lambda-\frac{1}{2}}(\cos\varepsilon) \approx 2(\varepsilon/\sin\varepsilon)^{1/2} J_1(\lambda\varepsilon)/\varepsilon,$$

$$t_{\lambda-\frac{1}{2}}(\cos\varepsilon) \approx 2(\varepsilon/\sin\varepsilon)^{1/2} \lambda J_1'(\lambda\varepsilon), \tag{17}$$

where $|\lambda|\sim\beta\gg1$, and J_1 is Bessel's function of order one. As we move away from the backward direction, the amplitudes decrease by a factor $\sim(\beta\sin\varepsilon)^{1/2}\sim\beta^{1/2}$ sufficiently far

away. Conversely, we can say that the amplitudes are enhanced by a factor of the order of $\beta^{1/2}$ as we approach the backward direction. This is Van de Hulst's axial focusing effect (Sect.3).

This effect has been experimentally observed[17,19,37] by placing a photographic plate behind the droplet in the near-field (Fresnel) region. The circumference of the droplet appears as a thin luminous line, and it has been verified that[19] this is more luminous than the reflected axial spot roughly in the ratio of (15) to (14) for $\beta \sim 10^2$. In fact, for $\beta \lesssim 80$, only the circumference remains visible: the axial spot is no longer seen[19]. The phenomenon may be likened to the luminosity of diffracting edges discussed by Sommerfeld[38].

v) Orbiting

Within the edge domain (8), the reflection coefficient in (6) is of the form

$$|\rho| = 1 - \delta \quad , \qquad \delta \sim b\beta^{-1/3} \quad , \tag{18}$$

where b is of order unity. We expect, therefore, that the amplitude of the pth Debye term is damped, for large p, by a factor of the order of

$$|\rho|^p = (1-\delta)^p \sim \exp(-p\delta). \tag{19}$$

A rough estimate of the number of contributing Debye terms would be, therefore, that it is of the order of $2/\delta$. This yields a value of the order of 50 for $\beta \sim 10^2$ and of the order of 100 for $\beta \sim 10^3$. These large numbers of internal reflections, as mentioned in Sect. 6, represent a kind of orbiting effect.

vi) Geometrical resonances

When paths involving large numbers of internal reflections close to the critical angle are considered, the possibility of "geometrical resonances"[11] associated with closed or nearly-closed orbits must be taken into account. The existence of such orbits leads to periodic or quasi-periodic features that play an important role in the theory, as will be seen below. The rapid variation of the glory pattern with N is related with

the closeness of approach to periodic orbits. In view of the reflection damping (19), only the lowest closed orbits need to be considered. For

$$N = [\cos(11\pi/48)]^{-1} \approx 1.33007, \tag{20}$$

a tangentially incident ray gives rise to a closed orbit, a regular star-shaped polygon of 48 sides inscribed within the droplet (fig. 6). The resulting periodicity with period 48 simplifies the discussion, so that the value (20) of N, which is within the range of variation of the refractive index of water in the visible spectrum, will be employed from now on.

9. Dominant Debye Terms and Their Physical Interpretation

What types of contributions from higher-order Debye terms do we expect to be dominant in the glory, and from which terms do they come? It suffices to consider the case of exactly backward scattering, $\theta = \pi$, and the contributions due to incident rays in the edge domain.

One type of contributions generated by such rays is that of surface waves, which we already know to be important for p=2 (van de Hulst's term). In view of the damping factor (9), we may restrict ourselves to those surface waves that emerge closest to the backward direction (within less than one short - cut). The corresponding total angle described along the surface is given by[11]

$$\zeta_p \equiv \pi - p\,\theta_t \pmod{2\pi},$$

$$0 \leq \zeta_p < \theta_t = 2\cos^{-1}(1/N), \tag{21}$$

and the relative surface-wave contribution of different Debye terms[11] should be the larger the lower the corresponding ζ_p, since the damping exponent, according to (9), is proportional to ζ_p (ignoring the additional reflection damping (19)).

For N given by (20), we have $\zeta_{24}=0$, corresponding in geometrical-optic terms to a higher-order "glory ray". This

actually means that, for p=24, the backward direction coincides with a geometrical shadow boundary from which further surface waves are launched, i.e., it lies on a Fock transition region (Sect. 7). Still disregarding reflection damping, we would expect p=24 to yield a dominant surface-wave type contribution, followed, in order of decreasing importance, by the values of p shown in the fourth quadrant of fig. 6 (p=37, 2, 15,...). Due to the exact geometrical periodicity associated with (20), further values of p are obtained by adding multiples of the period $\Delta p=48$. However, the effects of reflection damping (19), neglected above, become increasingly more important for higher p and may alter this ordering.

Apart from $p \equiv 24 \pmod{48}$, no other "glory rays" arise from the edge domain. However, we may ask about possible "back effects" at $\theta = \pi$ of rays emerging "beyond" $\theta = \pi$ (in terms of their total deflection angle). Although $\theta = \pi$ is then in a shadow region for these rays, they may still have sizable back effects if an intensity enhancement occurs close to their direction of emergence. This is precisely what happens[27] for directions close to a rainbow angle, where there is an amplitude enhancement by a factor of $\sim \beta^{1/6}$ (Sect. 7(v)).

The angle of incidence θ_{1R} associated with the rainbow in a Debye term of order p (rainbow of order p-1) is given by

$$\cos \theta_{1R} = [(N^2-1)/(p^2-1)]^{1/2}. \qquad (22)$$

For large p, this corresponds to incidence in the edge domain ($\theta_{1R} \longrightarrow \pi/2$). For rainbows that turn their dark side towards $\theta = \pi$, the rainbow angle $\theta_{R,p}$ associated with a Debye term of order p lies at a deviation $\varepsilon_{R,p} = \pi - \theta_{R,p}$ away from the backward direction, where

$$\varepsilon_{R,p} \approx |\zeta_p| - (N^2-1)^{1/2}/p \qquad (p \gg 1), \qquad (23)$$

and ζ_p is defined by (21), now extended to negative values. Thus, for large p, negative values of ζ_p represent approximately the deviation between $\theta = \pi$ and the rainbow angle for the pth Debye term.

On the shadow side of the rainbow, the amplitude becomes

exponentially damped, and the damping exponent at $\theta=\pi$ for large p is proportional to (cf. (11) and (25) below) $\beta(\varepsilon_{R,p}/p)^{3/2} \sim \beta(|\zeta_p|/p)^{3/2}$; thus, as p increases, the angular width of the rainbow region also increases, and the effect of the rainbow enhancement may be felt at larger deviations from the rainbow angle.

This leads us to expect that significant contributions to the glory from the shadow side of a rainbow occur in Debye terms of order p such that

$$\zeta_p \equiv \pi - p\theta_t \pmod{2\pi}, \quad -\theta_t \leq \zeta_p < 0, \tag{24}$$

and also that the relative importance of these contributions decreases as $|\zeta_p|/p$ increases. The corresponding values of p (modulo 48) are shown in the third quadrant of fig. 6, where the ordering is qualitatively indicated by the lengths of the arrows (p=46, 11, 33,...). Again, this disregards the effects of reflection damping.

In order to test the validity of our expectations, we have computed the contributions of different Debye terms to $|S^M(\beta)|^2$ and to $|S^E(\beta)|^2$ (cf. (13)) for β=150, 500 and 1,500, by numerical summation of the corresponding partial-wave expansions. The results are shown in fig. 7, where all terms that contribute up to ~0.1% are included. Inspection of this figure and of fig. 6 shows that the dominant p values, as well as their ordering, are generally in good agreement with the above discussion. Discrepancies are due to several factors that were not taken into account: (a) Reflection damping effects (19) affect the ordering: large p values are damped, favoring lower-p contributions. According to (18), the ordering is most strongly affected for low values of β. (b) For the rainbow terms, the deviation from the rainbow angle differs from $|\zeta_p|$ by the correction term in (23), which is significant for lower p: e.g., in fig. 6, the rainbow angle for p=11 lies only ~3° away from the backward direction, rather than ~7.5° away. It follows that p=11 should give the leading rainbow-type contribution to the glory. (c) For low β, the angular width of the transition regions increases,

so that lower-p values may prevail, in spite of larger damping parameters. Thus, for p=7, the backward direction lies deep inside the rainbow shadow for β =1,500, but it lies within the principal rainbow peak for β=150, so that the exponential damping (11) is not yet effective at this β .

10. Asymptotic Representation of the Dominant Terms

Our next task is to justify the physical interpretation that was proposed for the dominant Debye terms. For this purpose, the asymptotic representations obtained by the modified Watson transformation are compared with the exact solution in some typical cases.

i) Rainbow contributions

The Chester-Friedman-Ursell method mentioned in Sect. 7(v) may be applied not only to the primary bow[28], but also to a rainbow of arbitrary order. The magnetic rainbow contribution to the pth Debye term at $\theta = \pi$ (cf. (13)) is given by[27]

$$S^M_{p,R}(\beta) = i^{p+1}(-)^{(s+1)/2}\,\pi N K^{5/3}\exp(KA)$$

$$\times\left\{\left[p^M_{0,p} + O(K^{-1})\right]Ai(K^{2/3}\zeta) - K^{-1/3}\left[q^M_{0,p} + O(K^{-1})\right]Ai'(K^{2/3}\zeta)\right\}, \tag{25}$$

where $K = 2\beta$ and s is an integer; furthermore,

$$\left\{\begin{matrix} A \\ \frac{2}{3}\zeta^{3/2}\end{matrix}\right\} = \frac{i}{2}\left[pN(\cos\theta'_1 \pm \cos\theta''_1) - (\cos\theta'_2 \pm \cos\theta''_2)\right], \tag{26}$$

where $\bar\lambda' = \beta\sin\theta'_1 = N\beta\sin\theta'_2$ and $\bar\lambda'' = \beta\sin\theta''_1 = N\beta\sin\theta''_2$ are the two saddle points in the complex λ-plane (cf. (10)); the Chester-Friedman-Ursell coefficients $p^M_{0,p}$, $q^M_{0,p}$ are also determined by the saddle points. A similar expression is found for the electric contribution. Deep within the shadow side, one may employ (11) and, to first order in 1/p for large p, one finds $\zeta \approx |\zeta_p|/p$, yielding the damping exponent mentioned in Sect. 9.

In particular, for p= 11 (dominant rainbow contribution

to the glory), one gets

$$p^{M}_{0,11} \approx 1.1 \times 10^{-3} i \quad , \quad q^{M}_{0,11} \approx 1.5 \times 10^{-2},$$

$$p^{E}_{0,11} \approx 1.3 \times 10^{-4} i \quad , \quad q^{E}_{0,11} \approx 1.0 \times 10^{-2}, \qquad (27)$$

so that, unlike the situation found for the primary bow[28], the Airy approximation is inadequate for <u>both</u> polarizations. This is due to the sharp variation of the Fresnel reflection coefficients in the edge domain.

On the other hand, the magnetic rainbow contributions are larger than the electric ones for all p, as may also be noticed in fig. 7. This is so because the Fresnel reflection coefficient is always larger for magnetic (perpendicular) polarization.

Table I shows a comparison between the results from (25) and the exact partial-wave sum for p=11. The physical interpretation of this Debye contribution as a rainbow effect is clearly justified. The deviations arise from corrections not taken into account, including the effect of higher-order Chester-Friedman-Ursell coefficients.

ii) <u>Surface-wave contributions</u>

It is quite difficult to obtain accurate asymptotic representations of the surface-wave contributions for large p in manageable form, because they correspond to residues at Regge-Debye poles of order p+1. In general, one is led to representations in terms of Fock-type integrals (Sect. 7(iv)) which, when evaluated by residues, lead to these surface-wave contributions. One may take advantage of a "geometrical resonance", e.g. for N given by (20), to sum over the associated periodicity: for (20), this means summation over the period $\Delta p=48$. Due to the periodicity, the sum is over surface waves which all have the same damping angle ζ_p ($\zeta_{p'}=\zeta_p$ if $p' \equiv p \pmod{48}$).

The summation restores some features of the original Regge poles (before the Debye expansion): the resulting poles are all simple. Also, by suitably distorting the path of integration, only surface-wave-type poles contribute. However, the price one pays is that each Regge-Debye pole is replaced by a

cluster of simple poles (in the present case, 48 of them). The poles cluster around

$$\lambda_n = \beta + e^{i\pi/3}(\beta/2)^{1/3} x_n \quad , \tag{28}$$

where $-x_n$ is the nth zero of the Airy function.

For N given by (20), the residue contribution from the neighborhood of (28) associated with all Debye terms $p \equiv p_0$ (mod 48) is, at $\theta = \pi$,

$$(-)^{(s_0+1)/2} \exp(-i\pi/6)(\beta/2)^{4/3} \exp(-11 i\pi p_0/48) \exp(i\beta\zeta_p)$$

$$\times \frac{\eta}{48} \sum_{k=0}^{47} \exp(2i\pi p_0 k/48) \frac{\exp[i e^{i\pi/3} x_{n,k} (\beta/2)^{1/3} \zeta_p]}{A'^{\,2}_{n,k} + x_{n,k} A^2_{n,k}} \quad , \tag{29}$$

where s_0 is an integer, $\eta = 1$ for magnetic polarization and $\eta = N^2$ for electric polarization, $x_{n,k}$ is the solution near $x = x_n$ of

$$Ai'(-x)/Ai(-x) = -e^{i\pi/3}(N^2-1)^{1/2}/\eta\,(\beta/2)^{1/3}$$

$$\times \tan[(N^2-1)^{1/2}\beta - \pi(2k+13)/96] \quad , \tag{30}$$

and

$$A'_{n,k} = Ai'(-x_{n,k}) \quad , \qquad A_{n,k} = Ai(-x_{n,k}) \quad . \tag{31}$$

Within a cluster, the summands in (29) are slowly-varying, resulting in a considerable amount of cancellation among the terms, specially at large values of n. The magnitude of each term is comparable with that of Van de Hulst's term (15); in particular, as mentioned above, the associated damping exponent is of the order of $\beta^{1/3}\zeta_p$.

Numerical comparisons with the exact results were carried out for the "glory-ray" term $p_0 = 24$, for which $\zeta_p = 0$. For this purpose, the parent (Fock-type) integral from which (29) is derived was employed , retaining correction terms one order higher in $\beta^{-1/3}$. The results near $\beta = 1{,}500$ are given in Table II. Again, they show that the proposed physical interpretation of the associated Debye contributions is justified.

11. Discussion of the Glory Pattern

We can now interpret the results obtained in numerical studies of the glory pattern (Sect. 4) in terms of the dominant Debye contributions.

The glory pattern results from the interference among many Debye terms. For each term, rapid variations with β arise mainly from the phase factor associated with the corresponding optical path through the sphere. According to the above discussion, this optical path, for the pth term, is composed mainly of p shortcuts through the sphere at an angle of incidence close to the critical angle. Each shortcut contributes $2(N^2-1)^{1/2}\beta$ to the phase. If β changes by

$$\Delta\beta = 5\pi/(22\sqrt{N^2-1}) \approx 0.814 \tag{32}$$

for N given by (20), the phase of the dominant Debye terms in fig. 7 changes either by π or by an amount very close to π (mod 2π). Thus, we expect a quasi-periodic behavior (not an exact periodicity) with the quasi-period (32), which is in excellent agreement with the observed value (Sect. 4(i)).

Figs. 8 to 10 show the behavior of $|S^M(\beta)|^2$ within a quasi-period[39] near β =150, 500 and 1,500. In each case, the exact solution (curve in full line) is compared with the contribution from the two leading Debye terms in fig. 7 (dash-and-dot curve). We see that the interference between these terms, respectively the leading surface-wave term and the leading rainbow term, is responsible for the slowly-varying main humps within a quasi-period (Sect. 4(ii)).

When we include the contribution from all Debye terms indicated in fig. 6 (without summing over the period Δp=48), we reproduce (curve in broken line) most of the main features of the exact solution, except for the sharp superimposed spikes (Sect. 4(iii)). As more and more Debye terms are included, the approach to the exact result may be likened to the way a Fourier series approaches a periodic function.

Finally, when we carry out the summation over the period Δp=48, the spikes are recovered (fig. 10, inset). We conclude that the spikes are geometrical resonance effects associated with the quasi-periodic orbits with Δp=48 (cf. fig. 6), their

sharpness being due to the very long optical paths involved. It also follows that the spikes should be the first to disappear when absorption is taken into account by adding a small imaginary part to N. This has indeed been observed[17] (Sect. 4(iv)).

Both the spikes and the other interference oscillations occur at different values of β for $S^M(\beta)$ and $S^E(\beta)$, so that the total intensity $|S_1(\beta,\pi)|^2$ (cf. (13) shows additional structure due to the interference between magnetic and electric contributions (cross-polarization). One must also take into account the interference with the direct-reflection term (p=0), which has been omitted in figs. 8-10; its effect is small, except possibly at the minima.

Both the order of the leading Debye term and the nature of the leading contribution to the glory undergo considerable changes with β within the range of values of β for which glories are observed. The order of magnitude of the surface-wave contribution is exemplified by that of the Vande Hulst term (15), which yields, as a very rough estimate,

$$|S^M_{2,res}(\beta,\pi)|^2 \sim a\,\beta^{8/3}\exp(-b\,\beta^{1/3}), \tag{33}$$

with a and b of order unity. On the other hand, for p=11, the argument of the Airy functions in (25) is small ($\lesssim 1$) for $\beta \lesssim 10^4$, so that, taking into account (27), one finds, within this range of β,

$$|S^M_{11,R}(\beta,\pi)|^2 \sim c\,\beta^{10/3}\,(1+d\,\beta^{-2/3}), \tag{34}$$

where $c \sim 10^{-5}$, $d \sim 10^2$. It follows from (33) and (34) that, for β in this range, the magnetic contribution from p=2 dominates over that from p=11 for $\beta \sim 10^2$, but the reverse is already true for $\beta \sim 5\times10^2$, as is also clear from fig. 7. However, (34) only holds while $\theta = \pi$ is still close to the rainbow peak; as β increases to values $\gtrsim 10^4$, the width of the rainbow shrinks and $\theta = \pi$ gets deeper into the shadow, where the damping eventually becomes exponential in β (cf. (11)), i.e., stronger than that of (33). For still higher β, both terms eventually get damped below the geometrical-optic

contribution (14). On the other hand, according to (18), the effect of reflection damping in the edge domain decreases as β increases, so that it has less influence on the ordering of Debye contributions; thus, for $\beta = 1{,}500$, the ordering of magnetic terms is closer to that shown in fig. 6.

Now let us briefly discuss the angular distribution and polarization of the glory rings. We restrict ourselves to the domain where $u = \beta\varepsilon = \beta(\pi-\theta)$ is not $\gg 1$ (first few glory rings). Since both rainbow and surface-wave contributions arise from the neighborhood of $\lambda=\beta$ in the λ-plane, we may employ the asymptotic expansions (17) of the angular functions (with λ replaced by β). For small enough ε, the coefficients of these angular functions may be replaced, as a first approximation, by the values corresponding to $\varepsilon = 0$, i.e., by the two terms of (13), leading to

$$\frac{1}{2} S_1(\beta, \pi-\varepsilon) \approx S^M(\beta) J_1'(u) + S^E(\beta) J_1(u)/u, \quad u=\beta\varepsilon, \tag{35}$$

where J_1 is Bessel's function of order one; S_2 is obtained by interchanging M and E and changing the sign. A similar expression was given by Van de Hulst[7], whose coefficients c_1 and c_2 correspond to $2S^M$ and $2S^E$, respectively.

The angular distribution of the glory results from the interference between the two terms of (35). The squares of the two angular functions are plotted in fig. 11. Beyond its first zero, the contribution from $J_1(u)/u$ becomes very small, so that S_1 is dominated by magnetic contributions and S_2 by electric ones, as was mentioned in Sect. 4. Setting

$$i_j(\beta,\theta) = |S_j(\beta,\theta)|^2 \qquad (j = 1,2), \tag{36}$$

the total scattered intensity, for natural incident light (sunlight), is proportional to $i_1 + i_2$, and the degree of polarization of the scattered light is

$$P(\beta,\theta) = (i_1 - i_2)/(i_1 + i_2). \tag{37}$$

The angular distribution and polarization of the glory therefore depend on the relative magnitude and phase of $S^M(\beta)$ and

$S^E(\beta)$. Since both of them undergo considerable variations as a function of β, so do the angular distribution and the polarization, as was verified by Dave[18] (Sect. 4). The shape of the angular functions in fig. 11 shows that, if S^M and S^E are of comparable order of magnitude, the first dark ring will be hazy i.e., it will not correspond to a very large depression in the intensity, as has indeed been observed (Sect. 4). From (37) and fig. 11 we see also that the outer rings tend to be mainly perpendicular-polarized or mainly parallel-polarized depending on whether S^M or S^E predominates at the value of β under consideration; however, the polarization also varies with θ.

According to Sect. 10(i), magnetic polarization is dominant for rainbow contributions, whereas, according to (29), electric polarization would tend to dominate for surface-wave contributions. Since the leading contribution to the glory arises from surface waves for $\beta \sim 10^2$ and from rainbow terms for $\beta \sim 10^3$, it follows that the dominant polarization in the outer rings tends to be electric (parallel) for $\beta \sim 10^2$, changing over to magnetic (perpendicular) for $\beta \sim 10^3$. This agrees with observations quoted by Van de Hulst[7], as well as with Dave's[18] results (Sect.4).

Detailed computations of the scattered intensity in other directions have shown that it also undergoes rapid fluctuations as a function of β, although the amplitude of these fluctuations decreases rapidly as we move away from the backward direction. These "ripple" effects represent an attenuated version of the glory[11], and they may be treated in exactly similar terms. The same is true for the ripple in the total cross-section[40].

12. Conclusion

The glory is a highly intricate scattering effect, that results from a large number of physical effects acting together:

a) Edge effect: The glory is due to incident rays in the edge domain (8), i.e., close to the top of the barrier in the

effective potential - both above the top, corresponding to rays that hit the sphere within Fock's penumbra region, and below the top, corresponding to rays that reach the surface by barrier penetration.

b) "Orbiting": Such rays penetrate within the sphere close to the critical angle and undergo nearly-total internal reflection, so that they take many turns around the sphere before being appreciably damped - an effect related with orbiting. Thus, many higher-order Debye terms contribute.

c) Axial focusing: This is an amplitude enhancement by a factor $\sim \beta^{1/2}$ that arises from axial symmetry and from the peripheral nature of the leading contributions to the glory.

d) Cross-polarization: Interference between contributions of comparable magnitude from electric and magnetic polarizations leads to additional structure in the glory pattern.

e) Surface waves: This is one of the two types of leading contributions; it arises from Regge-Debye poles. Besides Van de Hulst's term, surface waves that have taken additional short-cuts through the sphere must also be included. Particularly important as a limiting case are "glory-ray" contributions, such as that from p=24 for N given by (20), which yields a Fock-type term.

f) Complex rainbow rays: The other type of leading contribution is that from complex rays on the shadow side of higher-order rainbows formed near the backward direction. These complex saddle-point contributions are important both due to the rainbow enhancement by $\sim \beta^{1/6}$ and due to the flattening of the rainbow peak for higher-order rainbows.

g) Geometrical resonances: Closed or nearly-closed quasi-periodic orbits are related both with the quasi-periodicity of the glory pattern and with the formation of very narrow resonances, the glory "spikes". As is well-known[31], periodic orbits play an important role in the semiclassical approach to quantization and in the tratment of bound states and resonances.

h) Competing damping effects: The evolution of the glory pattern and polarization as a function of β and θ reflects the interplay of several damping effects that compete to determine whether the leading term is electric or magnetic, of surface-

wave type or of rainbow-type, and the ordering of Debye contributions. Surface waves are damped by radiation in tangential directions, rainbow terms are damped as complex rays in the shadow of a caustic, and all terms are damped by the effect of multiple internal reflections. Surface-wave effects tend to predominate near $\beta \sim 10^2$ and rainbow effects are dominant near $\beta \sim 10^3$.

One or more of the above effects may play a significant role in other fields of physics. The glories that have been observed in atomic and molecular scattering[41] are usually due to the existence of glory rays, and the effect of axial focusing must be taken into account[42]. According to the above discussion, axial focusing is to be expected in processes dominated by peripheral interactions of high angular momentum. This situation is apparently found in nuclear scattering involving heavy ions; it has been suggested that surface waves, as well as complex saddle points, also play a role in this case[43].

The glory shows for the first time in optics that diffraction effects due to complex orbits (surface waves, complex rainbow rays) may be strongly dominant over geometrical-optic ray contributions (real orbits). The moral this suggests is that complex extremals of Feynman path integrals may have to be taken into account in more general situations[31,44,45].

TABLE I - Comparison between $S_{11}^{M}(\beta,\pi)$ (exact) and $S_{11,R}^{M}(\beta)$ ("rainbow" term)

β	Exact	Asymptotic
1,500.1	-333 - 794i	-304 - 823i
1,500.2	860 - 43i	878 - 8i
1,500.3	-249 + 824i	-289 + 829i
1,500.4	-690 - 514i	-681 - 553i
1,500.5	719 - 474i	752 - 454i

TABLE II - Comparison between $S_{24}^{M}(\beta,\pi)$ (exact) and the "surface-wave" term (both summed over $\Delta p=48$)

β	Exact	Asymptotic
1,500.1	183 - 231i	214 - 193i
1,500.2	-250 - 102i	-245 - 111i
1,500.3	52 + 244i	38 + 255i
1,500.4	205 - 187i	229 - 178i
1,500.5	-254 - 117i	-236 - 131i

FOOTNOTES AND REFERENCES

*Work partially supported by the National Research Council of Brazil.

1 J.M.Pernter and F.M.Exner, Meteorologische Optik, W.Braumüller, Vienna (1910).
2 A.Hayter, A Voyage in Vain, Faber and Faber, London We are indebted to Prof. J.B.French for this reference.
3 The Autobiography of Benvenuto Cellini, Chapter 128, Brentano's, New York (1906).
4 R.A.R.Tricker, Introduction to Meteorological Optics, American Elsevier Publishing Co., New York (1970).
5 J.C.Brandt, Publ.Astron.Soc.Pacific 80, 25 (1968); H.C. Bryant and N.Jarmie, Scient.Amer. 231, 60 (July 1974).
6 C.T.R.Wilson, Nobel Prize Lecture (1927).
7 H.C.Van de Hulst, Light Scattering by Small Particles, John Wiley and Sons, New York (1957).
8 G.Mie, Ann.Physik 25, 377 (1908).
9 V.Khare and H.M.Nussenzveig, to appear in Phys.Rev.Lett.
10 B.Ray, Nature 111, 183 (1923).
11 H.M.Nussenzveig, J.Math.Phys. 10, 82, 125 (1969).
12 H.C.Bryant and A.J.Cox, J.Opt.Soc.Am. 56, 1529 (1966).
13 J.Bricard, Ann.Physique 14, 148 (1940), Handb.d.Phys. 48, 351, Springer-Verlag, Berlin (1957).
14 H.Bucerius, Optik 1, 188 (1946).
15 H.C.Van de Hulst, J.Opt.Soc.Am. 37, 16 (1947); see also ref. 7.
16 H.Ott,Ann.Physik 41, 443 (1942), 4, 432 (1948).
17 T.S.Fahlen and H.C.Bryant, J.Opt.Soc.Am. 58, 304 (1968).
18 J.V.Dave, Appl.Opt.8, 155 (1969).
19 M.J.Saunders, J.Opt.Soc.Am. 60, 1359 (1970).
20 For the early history of this subject, see N.A.Logan, Proc. IEEE 53, 773 (1965).
21 V.A.Fock, Diffraction of Radio Waves around the Earth's Surface, Publishers of the USSR Academy of Sciences, Moscow (1946).
22 H.Bremmer, Terrestrial Radio Waves, Elsevier, New York (1949).
23 B.Van der Pol and H.Bremmer, Phil.Mag. 24, 141, 825 (1937).
24 W.Franz, Theorie der Beugung Elektromagnetischer Wellen, Springer-Verlag, Berlin (1957).
25 S.I.Rubinow, Ann.Phys. (N.Y.) 14, 305 (1961).
26 H.M.Nussenzveig, Ann.Phys. (N.Y.) 34, 23 (1965).
27 V.Khare, Ph. D.Thesis, University of Rochester (1975); V.Khare and H.M.Nussenzveig, to be published.
28 V.Khare and H.M.Nussenzveig, Phys.Rev.Lett. 33, 976 (1974).
29 H.M.Nussenzveig, in Methods and Problems of Theoretical Physics, J.E.Bowcock ed., North-Holland Publishing Co., Amsterdam (1970), p.203.
30 E.C.Titchmarsh, Introduction to the Theory of Fourier Integrals, 2nd ed., Oxford University Press (1937), p.60.
31 M.V.Berry and K.E.Mount, Rep.Prog.Phys. 35, 315 (1972).
32 J.B.Keller, in Proc.Symp.Appl.Math., vol.8, L.M.Graves ed., McGraw-Hill, New York (1958), p.27.

33 P.J.Debye, Physik. Z.9, 775 (1908).

34 K.W.Ford, D.L.Hill, M.Wakano and J.A.Wheeler,Ann.Phys. (N.Y.) 7, 239 (1959).

35 C.Chester, B.Friedman and F.Ursell, Proc.Camb.Phil.Soc. 53, 599 (1957); F.Ursell, Proc.Camb.Phil.Soc.61, 113 (1965).

36 H.M.Nussenzveig, Scient.Amer. 236, 116 (April 1977)

37 T.S.Fahlen and H.C.Bryant, J.Opt.Soc.Am. 56, 1635 (1966).

38 A.Sommerfeld, Optics, Academic Press Inc., New York (1954), p.262.

39 The direct-reflection term p=0 is omitted in all curves. This does not affect the comparison.

40 P.Walstra, Proc.Koninkl.Akad.Wetensch. B67, 491 (1964).

41 M.A.D.Fluendy and K.P.Lawley, Chemical Applications of Molecular Beam Scattering, Chapman and Hall, London (197).

42 M.V.Berry, J.Phys.B2, 381 (1969).

43 H.L.Harney, P.Braun-Munzinger and C.K.Gelbke, eds., Classical and Quantum-Mechanical Aspects of Heavy-Ion Collisions, Springer-Verlag, Berlin (1975); cf. specially the contributions by W.E.Frahn and K.W.McVoy and the references quoted therein.

44 W.H.Miller, Adv.Chem.Phys. 25, 63 (1974); T.F.George and J.Ross, Ann. Rev. Phys. Chem. 24, 263 (1973).

45 C.G.Callan, Jr., R.F.Dashen and D.J.Gross, Phys.Lett. 63B 334 (1976).

FIGURE CAPTIONS

FIG. 1 - An incident beam associated with the plane wave front ii' around a "glory ray" ABCDE is transmitted, after one internal reflection, as a diverging pencil (tt' = transmitted wave front) with a virtual focus at F. Due to axial symmetry for backscattering, the locus of virtual foci is the focal circle FF', which generates toroidal wave fronts, giving rise to the axial focusing effect .

FIG. 2 - According to Van de Hulst's conjecture, the glory would be due to tangentially incident rays penetrating at the critical angle θ_{ℓ} and taking two shortcuts AB and CD, linked by pieces of surface waves such as T_1A + BC + DT_2. The total angle $\alpha+\beta+\gamma$ described by the surface waves would be $\simeq 14^{\circ}$.

FIG. 3 - The effective potential seen by a partial wave is the sum of a square well with the corresponding centrifugal potential, giving rise to a barrier with a cusp at the top. The edge domain (8) corresponds to values of the angular momentum λ such that the energy E is within a small neighborhood of the top of the barrier.

FIG. 4 - The two types of "vertices" associated with the interaction of a critically incident ray with the surface of the sphere. The angle φ described as a surface wave may have any value.

FIG. 5 - Behavior of the saddle points in the λ-plane around a rainbow angle θ_R. As θ approaches θ_R from the lit side, two real saddle points (real rays) approach each other, colliding at $\theta = \theta_R$ and moving away along complex-conjugate directions for θ on the dark side. The complex ray on the dark side arises from the lower complex saddle point.

FIG. 6 - Path of a tangentially incident ray for N given by (20). The values of p at each vertex are indicated next to

the arrows, which point in directions corresponding to the angles ζ_p in (21) and (24) (e.g., $\zeta_{11}=-7.5^\circ$). ——— rainbow terms; ----- surface-wave terms. The ordering of terms by increasing ζ_p (surface waves) or $|\zeta_p|/p$ (rainbow terms) is qualitatively indicated by the lengths of the arrows. The actual rainbow angles $\theta_{R,p}$ are somewhat shifted from the corresponding $|\zeta_p|$. The direction corresponding to $\theta_{R,11}$ is indicated; since $\varepsilon_{R,11}/11 < \varepsilon_{R,46}/46$, the ordering is inverted in this case, and p=11 is the leading rainbow contribution.

FIG. 7 - Contributions from Debye terms of various orders to $|S^M(\beta)|^2$ and to $|S^E(\beta)|^2$ for β=150, 500 and 1,500: ——— rainbow terms; ----- surface-wave terms. All terms contributing up to 0.1% are shown. For β=150, there appear some terms not indicated in fig. 6 (shown by -.-.-).

FIG. 8 - Behavior of $|S^M(\beta)|^2$ within a quasi-period near β=150; ——— exact; -.-.- contribution from the two leading Debye terms in fig. 7; ---- contribution from all Debye terms indicated in fig. 6 (without summation over $\Delta p = 48$).

FIG. 9 - Same as fig. 8, near $\beta = 500$.

FIG. 10 - Same as fig. 8, near $\beta = 1{,}500$. The spike marked A is amplified in the inset, which shows the effect of summing over the period $\Delta p = 48$ on the approach to this spike: —— exact; ----- contribution from all Debye terms indicated in fig. 6 summed over $\Delta p = 48$.

FIG. 11 - Squares of the angular functions appearing in (35) as functions of u.

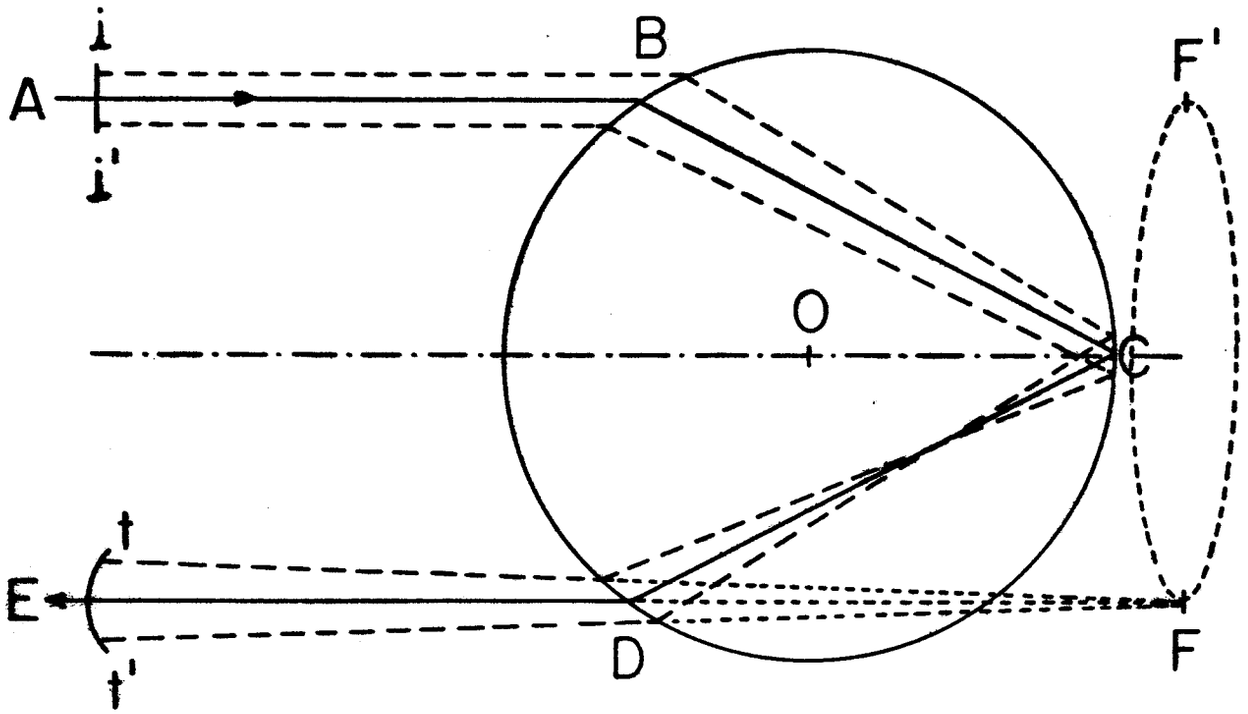

Fig. 1

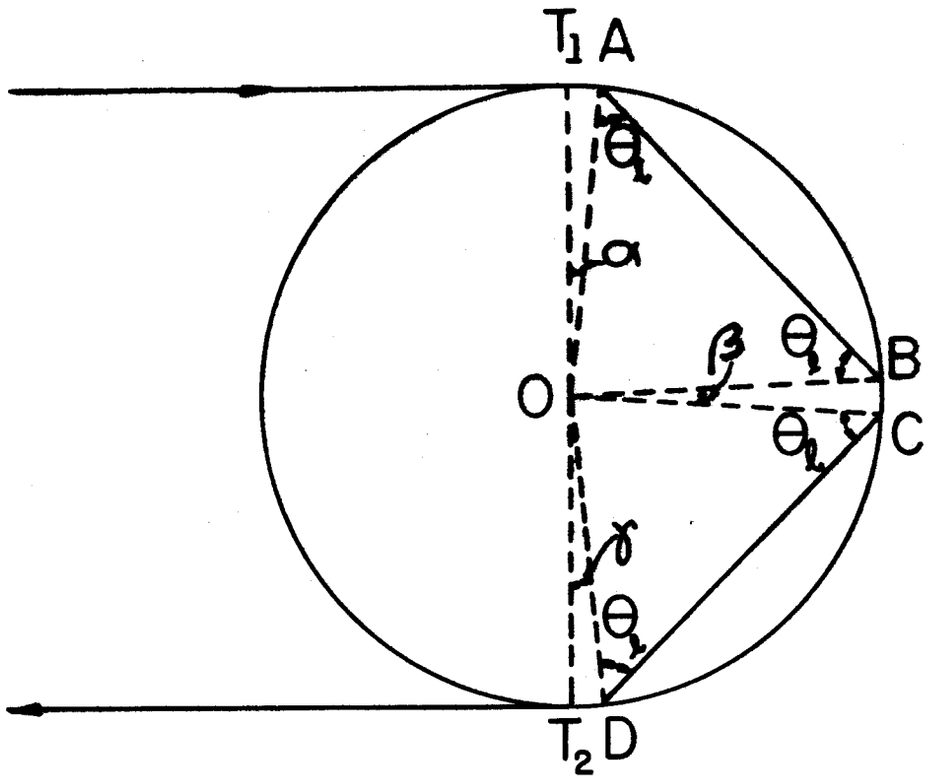

Fig. 2

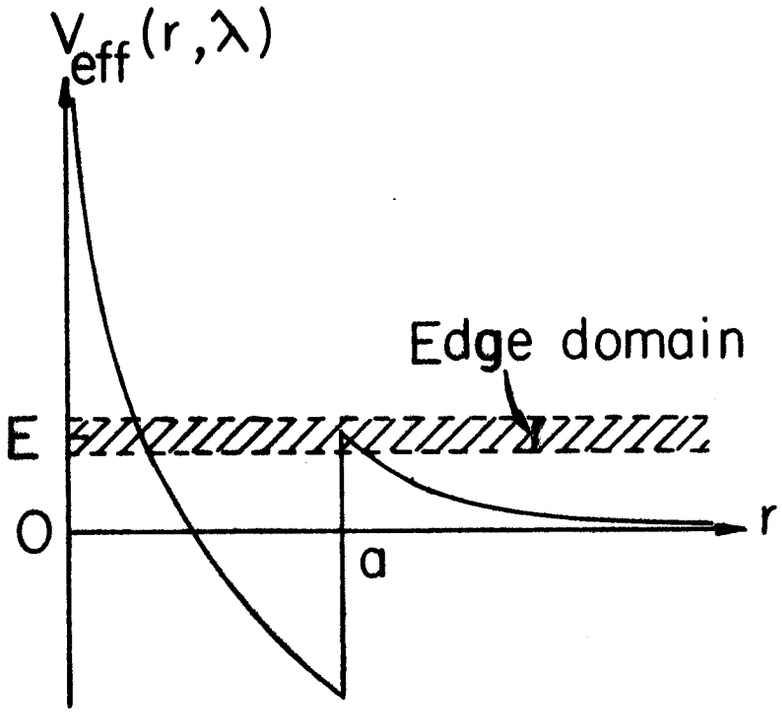

Fig. 3

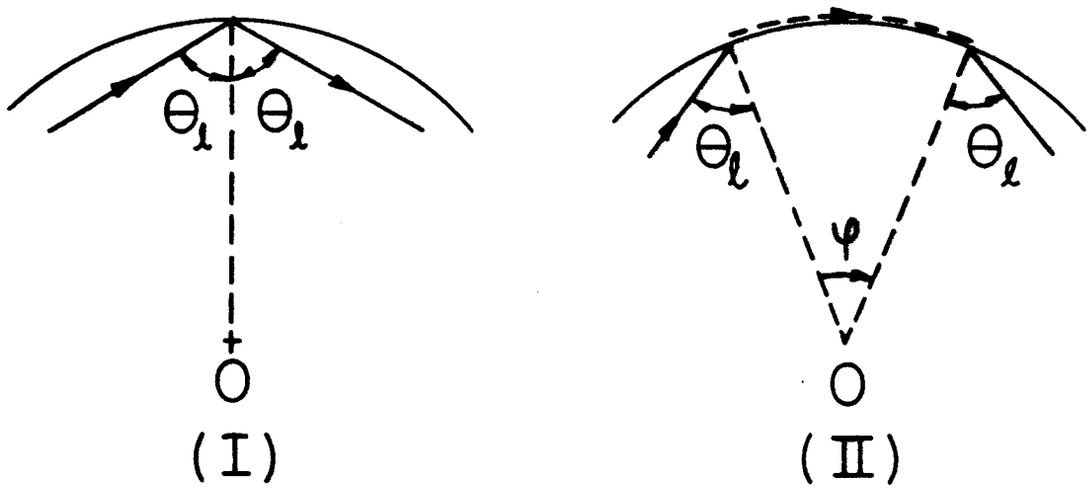

Fig. 4

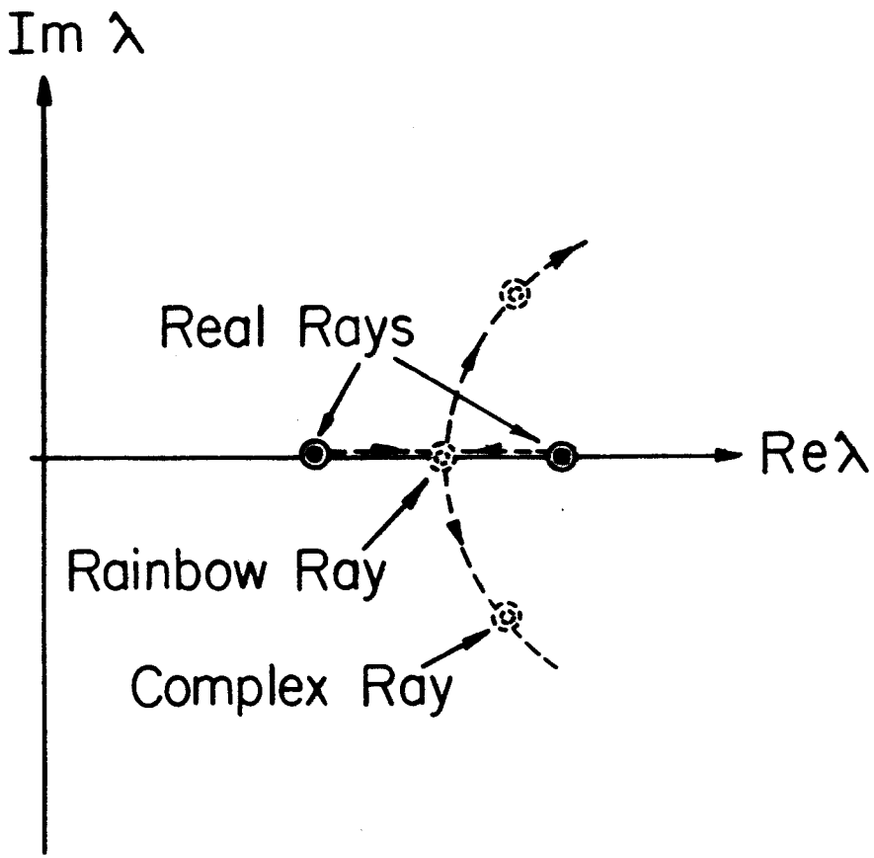

Fig. 5

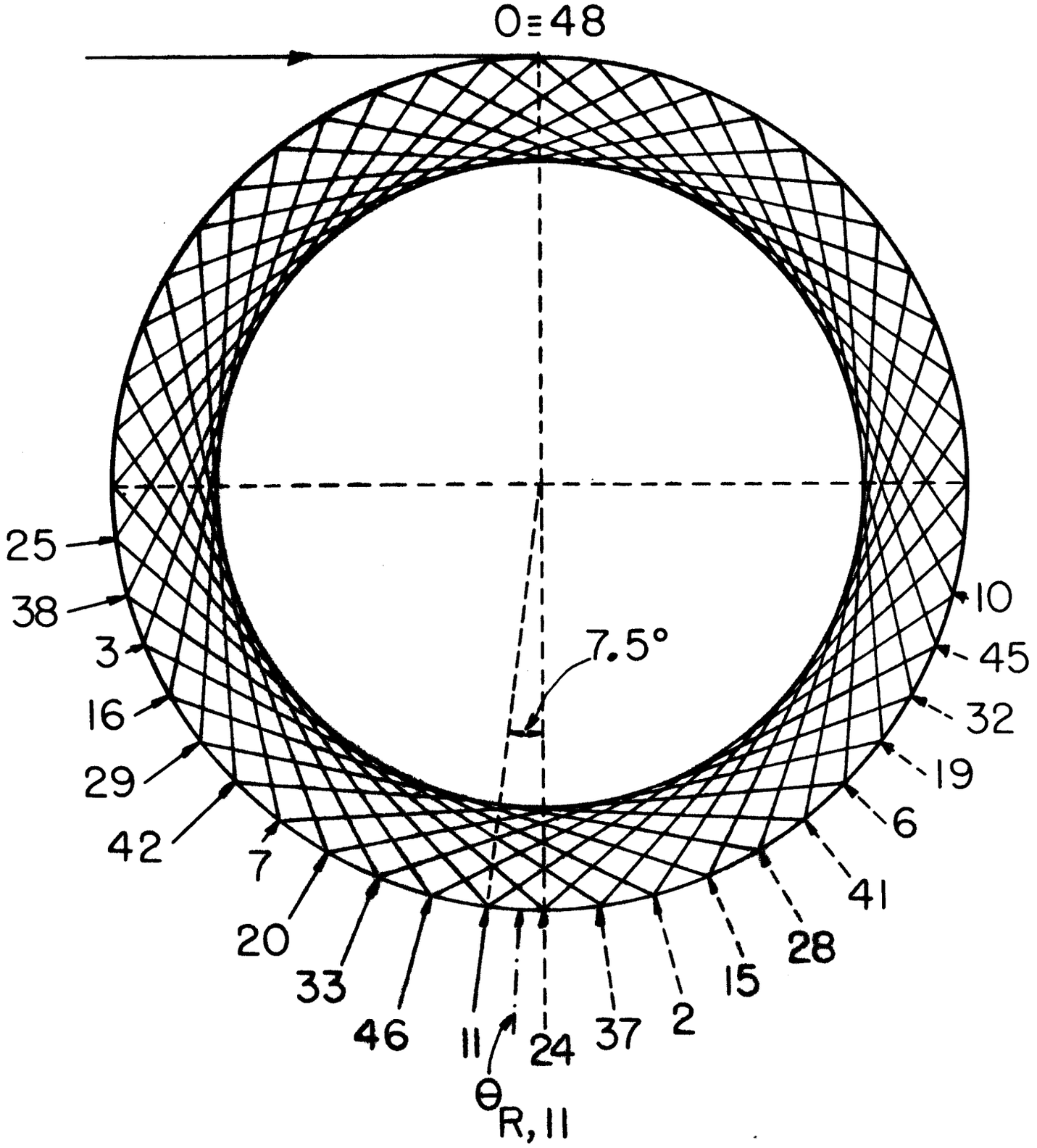
0≡48
25
38
3
16
29
42
7
20
33
46
11
24
37
2
15
28
41
6
19
32
45
10
7.5°
$\theta_{R,11}$

Fig. 6

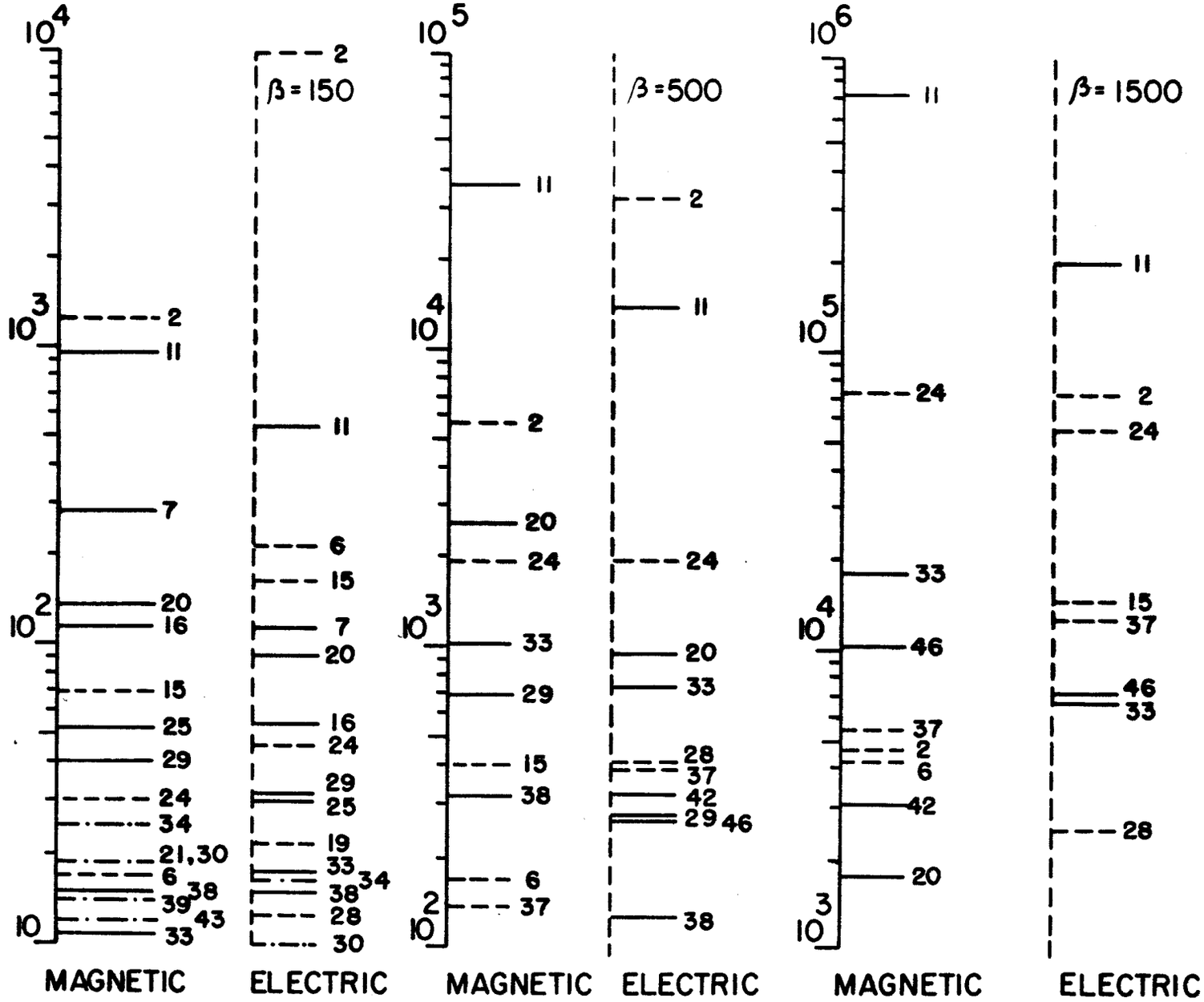
10^4
2
11
7
20
16
15
25
29
24
34
21,30
6
38
39
43
33
10^3
10^2
10
MAGNETIC
$\beta = 150$
2
11
6
15
7
20
16
24
29
25
19
33
34
38
38
28
30
ELECTRIC
10^5
11
2
20
24
33
29
15
38
6
37
10^4
10^3
10^2
MAGNETIC
$\beta = 500$
2
11
24
20
33
28
37
42
29
46
38
ELECTRIC
10^6
11
24
33
46
37
2
6
42
20
28
10^5
10^4
10^3
MAGNETIC
$\beta = 1500$
11
2
24
15
37
46
33
28
ELECTRIC

Fig. 7

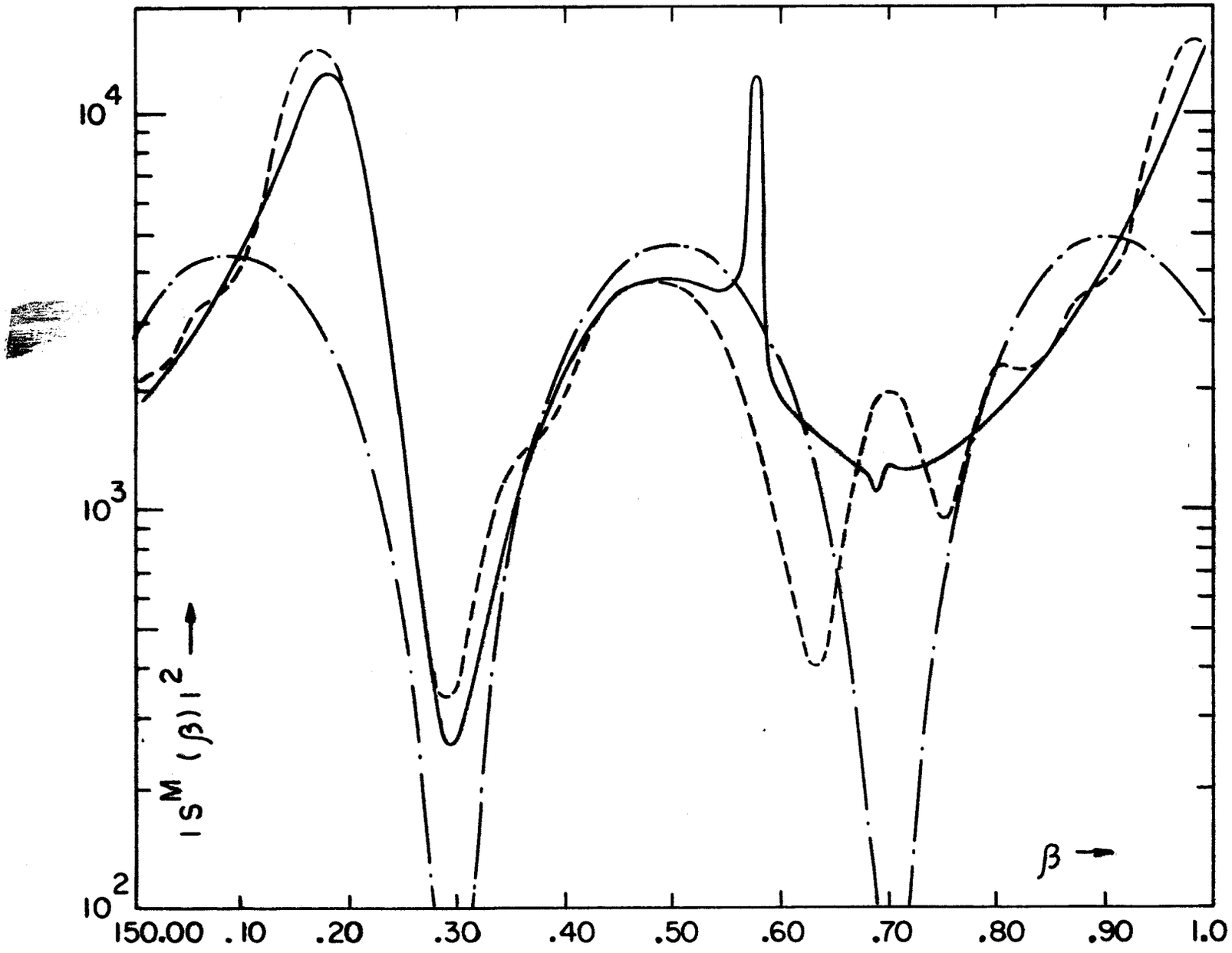

Fig. 8

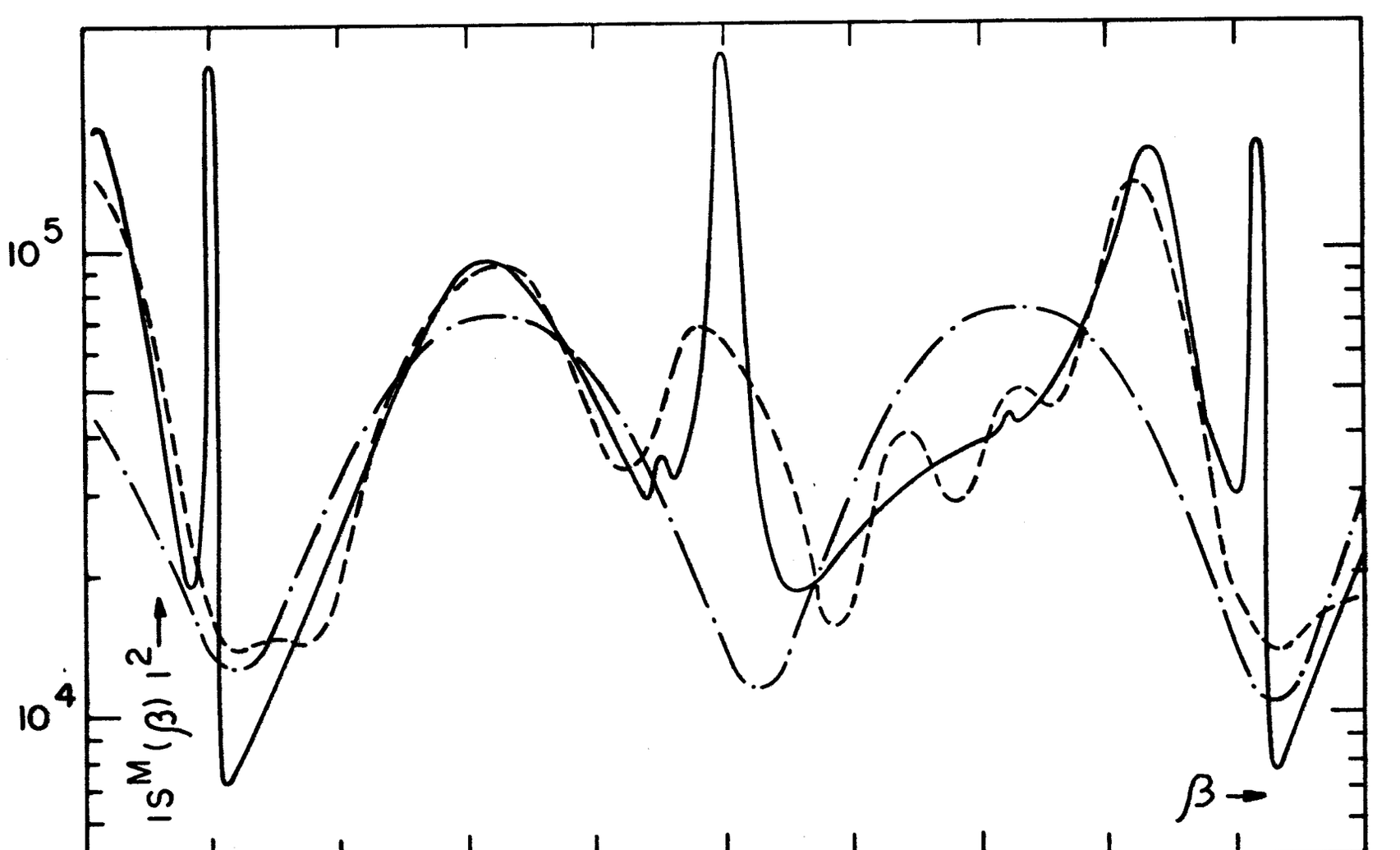

Fig.9

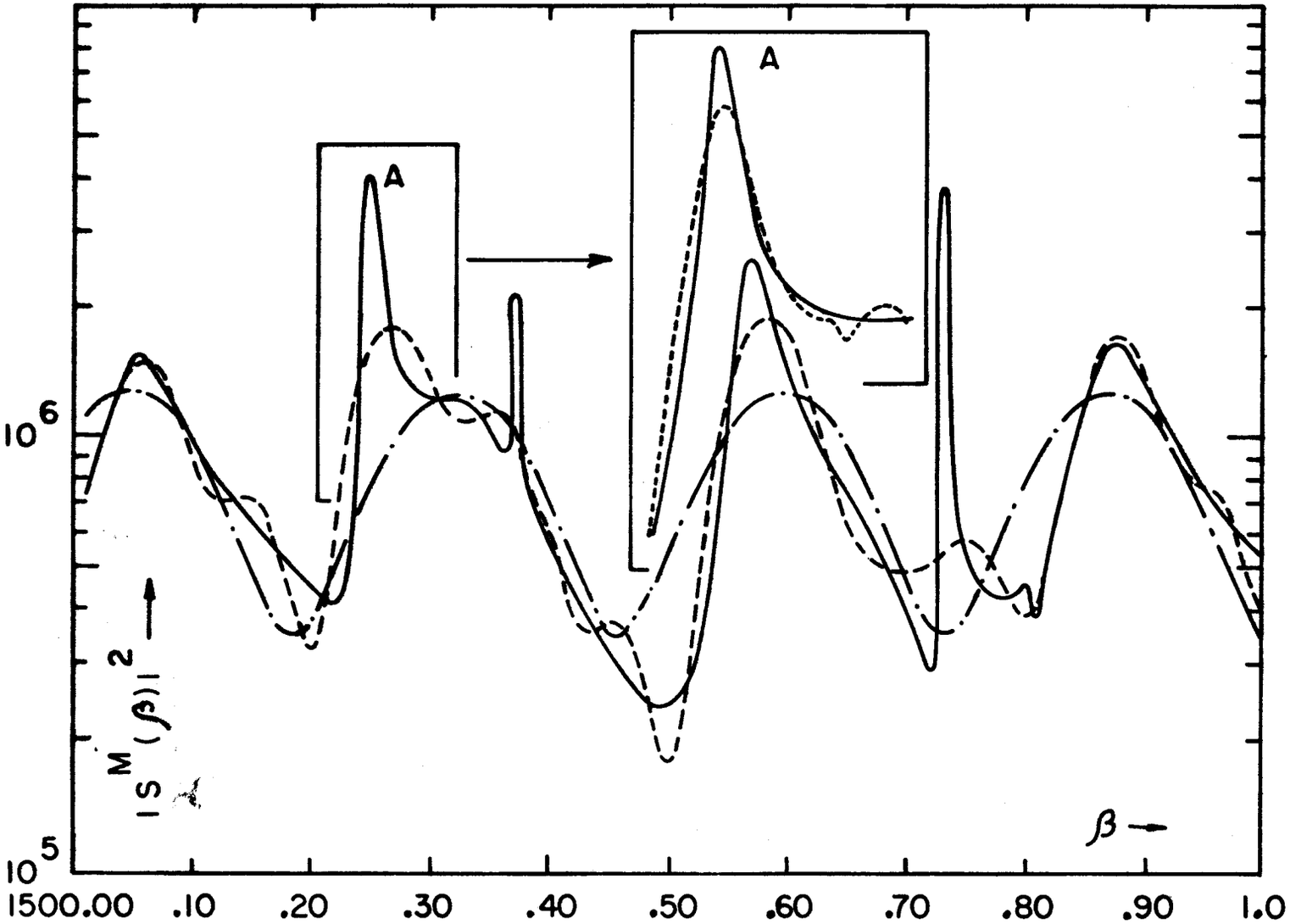

Fig. 10

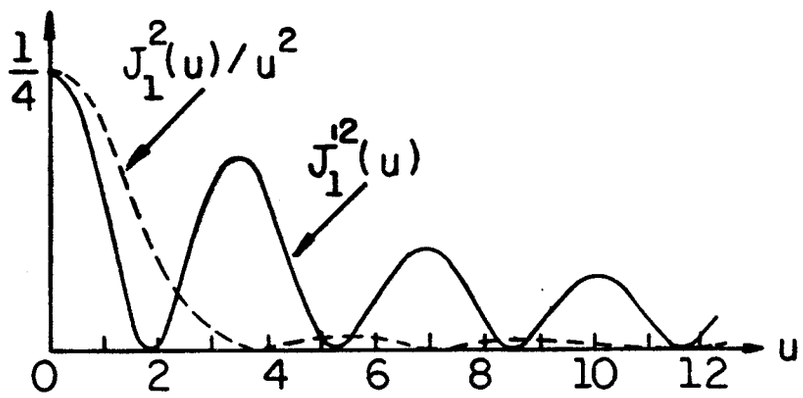

Fig. 11